Nuclear Structure Effects in Fission

S Åberg[1], M Albertsson[1], BG Carlsson[1], T Døssing[2], P Möller[1] and J Randrup[3]

[1] Mathematical Physics, Lund University, S-221 00 Lund, Sweden
[2] Niels Bohr Institute, DK-2100 Copenhagen Ø, Denmark
[3] Nuclear Science Division, Lawrence Berkeley National Laboratory, Berkeley, California 94720, USA

E-mail: sven.aberg@matfys.lth.se

Abstract. Three examples of nuclear structure effects in fission dynamics are discussed: (i) The appearance of a super-short symmetric mode in the fission of nuclei around ^{264}Fm leading to two double-magic ^{132}Sn, (ii) Fission of some super-heavy elements where the heavy cluster is focused around double-magic ^{208}Pb, and (iii) A saw-tooth distribution in angular momenta versus the fission fragment mass in the fission of ^{239}U. The Metropolis random walk method is used to simulate the strongly damped fission dynamics on a 5D deformation grid. The dynamics is driven by pairing-, shape- and energy-dependent level densities. When available, a good agreement with experimental data is obtained.

1. Introduction

Nuclear fission constitutes an extremely complex many-body problem where the nuclear shape dynamically undergoes a dramatic change from the ground-state shape to the point of scission where the nucleus splits into two fragments. The process is governed by a competition between the attractive strong nuclear force and the repulsive coulomb interaction between nucleons, and may be induced spontaneously or through a process where energy is added. The dynamical process implies large fluctuations and all observables are connected with certain distributions.

Nuclear structure plays an important role at several stages of the fission process, determining the mass division, the distribution of the total kinetic energy (TKE), the neutron evaporation from each fission fragment, and the angular momenta of the fragments. In this contribution we shall discuss consequences of shell structure in some cases, and compare to experimental data where it is available.

The dynamical evolution from the ground-state region to the scission shape is treated as an over-damped, Brownian process on a 5D potential-energy surface [1]. Shape-, energy- and angular momentum-dependent microscopic state densities [2] are calculated and used to guide the random walk [3], to determine the energy partition between the proto fragments [4], to determine the angular momenta of the two fragments [5], and finally, to determine the neutron evaporation multiplicity that occurs after the scission shapes are equilibrated to ground-state shapes. The applied mean-field model [6] that underlies each step of the calculations has been shown to provide a good global description of nuclear structure effects.

The nuclear shape is described by the five deformation degrees of freedom: elongation, mass asymmetry, deformation of each of the two fragments, and the neck radius. In the

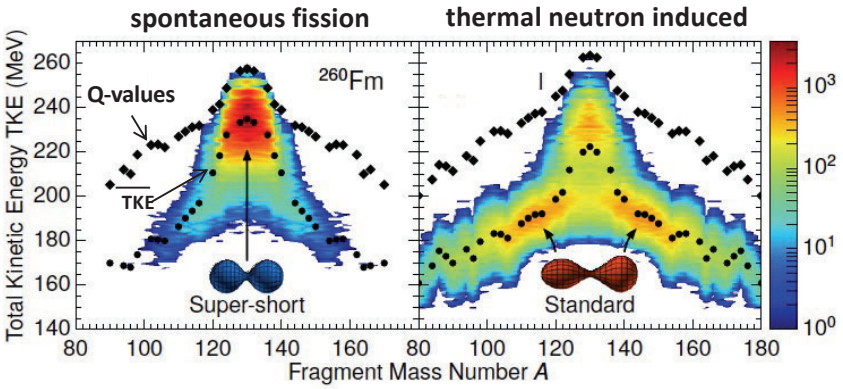

Figure 1. Total kinetic energy (TKE) versus fragment mass number for 10^5 calculated scission events of spontaneous fission (left-hand part) and thermal neutron induced fission events (right-hand part) of 260Fm. Black filled diamonds show Q*-values of each reaction, and black filled circles show calculated average values of TKE. Typical scission shapes at the two energies, Super-short and Standard, are shown. (From [7]).

dynamical process scission is assumed when the neck radius has become c_{crit} = 1.5 fm. At this stage the internal excitation energy is divided between the two fragments according to their microscopic state densities calculated at the scission shapes [7]. This gives a distribution of excitation energy that is sensitive to shell structure of both fragments at non-equilibrium shapes. Also the angular momenta are determined at this step where the angular momenta of the fragments are restricted to directions perpendicular to the symmetry axis of the fissioning nucleus at scission [5, 8]. The Coulomb interaction causes the two fragments to strongly repel each other and the total kinetic energy (TKE) is registered. Far apart the shapes of the two fragments are relaxed to equilibrium shapes causing a distortion energy. The excitation energy together with the distortion energy provides a total excitation energy of each fragment, $\mathrm{TXE}_{L/H}=\mathrm{E}_{exc,L/H}+\mathrm{E}_{dist,L/H}$. This energy allows the emission of a number of neutrons from each fragment, registered as the neutron multiplicity (followed by a number of emitted gamma-rays). The Q-value related to specific fission fragments (and a possible initial excitation energy) Q* relates to the TKE and $\mathrm{TXE}=\mathrm{TXE}_L+\mathrm{TXE}_H$ as Q*=TKE+TXE. For specific fragments an increased TKE thus implies a decreased TXE, i.e. a decrease in neutron multiplicity.

2. Results

We discuss three situations of fission dynamics where shell structure plays an important role. In Section 2.1 we describe how a super-short symmetric fission mode appears in fission dynamics of heavy Fm nuclei leading to symmetric fragments around the double-magic ^{132}Sn. The clustering of the heavy fission fragment around ^{208}Pb is suggested to occur in the fission of several super-heavy nuclei as described in Section 2.2. In Section 2.3 we discuss the observed [9] appearance of a saw-tooth behaviour of the average angular momentum carried by the fission fragments.

2.1. Super-short fission mode – role of ^{132}Sn

Calculated TKE-values versus fragment mass number at scission are shown in Fig. 1 in the case of spontaneous fission (SF; left-hand part) and thermal neutron induced fission (right-hand part) of ^{260}Fm (for details of the calculations see [7]). For SF most events occur with a symmetric fission fragment distribution in a super-short mode: both fragments are close to double-magic ^{132}Sn implying a scission configuration composed by two close-lying approximately spherical fragments. The close distance between the fragments implies a high average TKE, $\overline{\mathrm{TKE}}$ ≈230 MeV. With an increase of the excitation energy to 6.13 MeV, corresponding to the neutron separation energy, the picture is radically changed. The majority of the events now fission with an asymmetric mass distribution with the fragments more elongated. This implies in average a

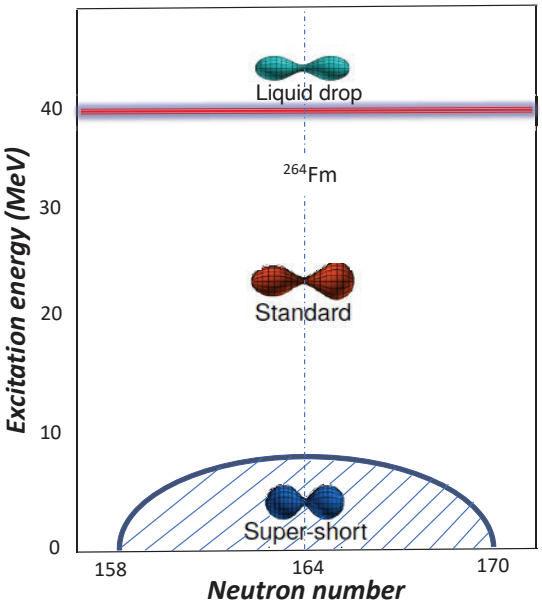

Figure 2. Phase diagram showing the appearance of three different modes occurring at different excitation energies in the fission of Fm isotopes. The super-short mode appears at low excitation energies in isotopes $^{258-270}$Fm. The mode is fragile and disappears as energy is slightly increased, and is replaced by the standard mode. At high excitation energies shell effects disappear and all nuclei fission in a symmetric liquid-drop way.

considerably lower total kinetic energy, $\overline{\mathrm{TKE}}$ ≈190 MeV.

For SF of ^{260}Fm the typical available TXE is small, $\overline{\mathrm{TXE}} \approx$ 22 MeV, as can be seen as the energy difference between the Q*-values and the $\overline{\mathrm{TKE}}$ in left-hand part of Fig. 1, leading to a calculated small average neutron multiplicity $\bar{\nu}$=2.9. The $\overline{\mathrm{TXE}}$ becomes large when fission is induced by thermal neutrons (right-hand part of Fig. 1) $\overline{\mathrm{TXE}} \approx$ 43 MeV, implying a much larger neutron multiplicity, $\bar{\nu}$=5.2 [7].

Considering the even Fm isotopes from mass number A=254-268 we find that spontaneous fission occurs in the standard mode for ^{256}Fm and lighter isotopes, it is bimodal in ^{258}Fm (with 55% in super-short mode), while for isotopes ^{260}Fm and heavier the fission takes place in the super-short fission mode. Increasing the excitation energy, by initiating the fission process by thermal neutrons on the odd neighbouring isotope, the transition to the super-short mode is delayed and begins at N=162, ^{262}Fm. By further increasing the excitation energy to 15 MeV all Fm isotopes are calculated to fission in the standard mode. If the excitation energy is substantially increased to about 40 MeV fission takes place in a third mode, the liquid-drop mode. Shell effects are then strongly diluted and the dynamics is determined by the energy variation of the liquid drop and level densities by the Fermi gas, implying symmetric fission with fairly elongated fragments. The calculated appearance of the three fission modes, super-short, standard and liquid drop in Fm isotopes are shown in the "phase diagram" Fig. 2.

It is interesting to investigate what causes the transition from the super-short fission mode at zero excitation energy to the standard fission mode at 6.13 MeV excitation energy. In Fig. 3 the potential energy of the two fission paths is plotted versus the elongation q_2 for ^{260}Fm. The remaining four deformation parameters are implicitly accounted for. The energy of the ridge separating the two paths is shown by the solid red line. Energywise the super-short path is open from the second minimum at SF while an excitation energy of about 4 MeV is needed to overcome the barrier to the standard mode. This implies a complete dominance of the super-short fission channel for SF, shown by the blue arrows. Thermal neutron induced fission implies an excitation

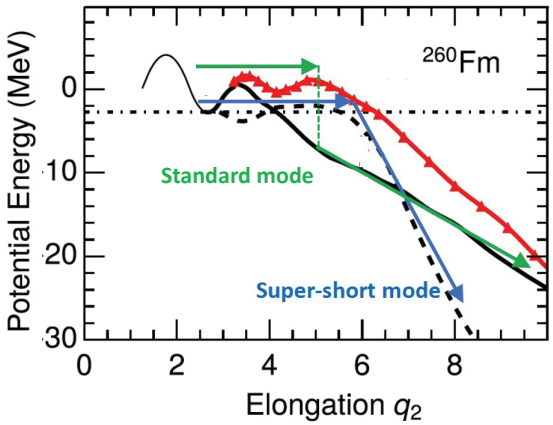

Figure 3. Potential-energy curves versus elongation for the two fission modes in ^{260}Fm, standard mode (solid black) and super-short (dashed solid). The two paths are separated by a ridge (red line). A dot-dashed horizontal line shows the ground-state energy. Typical fission paths at lower and higher energies are illustrated by blue and green arrows, respectively. (Partly from [7]).

energy of about 6 MeV and transitions to the standard path are possible in the random walk calculations. Transitions happens in particular for elongations around q_2=4-6 where the energy curve of the super-short mode is flat. The dynamics becomes diffusive and a relatively long time is spent at these elongations (many steps in the random walk), implying several chances to overcome the ridge towards the standard mode. Once such a transition is made (green arrows), the motion towards scission along the standard mode is fast due to the large energy slope of the potential-energy curve at these q_2 values. This results in a dominance of fission events along the standard path at excitation energies corresponding to the neutron binding energy.

The transition between the super-short mode to the standard mode of fission is thus due to shell structure and dynamical processes in the potential energy surface - there are no (or ignorable) changes of shell energies due to this small excitation energy.

The fission mode selected by the nucleus strongly affects several physical observables: the TKE, the fission fragment mass distribution, and also the neutron multiplicity. The suggested scenario with changes of fission mode with neutron number and change of mode with increasing excitation energy is supported by several sets of data, see [7] for more details.

2.2. Super-asymmetric fission mode – role of ^{208}Pb

In fission of super-heavy nuclei a clustering of the heavy fission fragment around ^{208}Pb may appear due to nuclear structure effects. In previous calculations [10] this was found to appear for several super-heavy nuclei, $^{274-286}$Cn, $^{272-284}$Ds and $^{272-276}$Hs. With the heavy fragment mass A_H ≈208 the mass of the light fission cluster, A_L, adjusts as the mass of the superheavy nucleus changes. One example is the fission of ^{274}Hs, and in Fig. 4 we show calculated TKE versus fragment number at scission at two excitation energies 6.7 MeV (left-hand part) and 10 MeV (right-hand part). At the lower energy the heavy fragment has a peak around A_H=208 and the lighter fragment around A_L=66, *i.e.* fission occurs in a super-asymmetric mode due to strong shell effects from ^{208}Pb. When the energy is slightly increased to 10 MeV the picture is changed completely and the fission fragments obtain a symmetric mass distribution. The understanding of this drastic change of fission mode is similar to what was discussed for ^{260}Fm in last subsection [11].

At 6.7 MeV we obtain a quite small $\overline{\mathrm{TXE}} \approx 20$ MeV ($\overline{\mathrm{TXE}} = \mathrm{Q}^* - \overline{\mathrm{TKE}}$), while at 10 MeV it is radically larger, $\overline{\mathrm{TXE}}$ ≈90 MeV, see Fig. 4. This leads to a dramatic increase in the average neutron multiplicity from about $\bar{\nu}$= 2.5 to $\bar{\nu}$= 7.7 as the energy is increased by 3.3 MeV [11]. This can be compared to the neutron multiplicity increase from $\bar{\nu}$=1.5 to $\bar{\nu}$=2.5 as energy is increased from 0 to 6.7 MeV. Indeed, the change of fission mode from super-asymmetric to symmetric is found to imply a huge increase in neutron multiplicity.

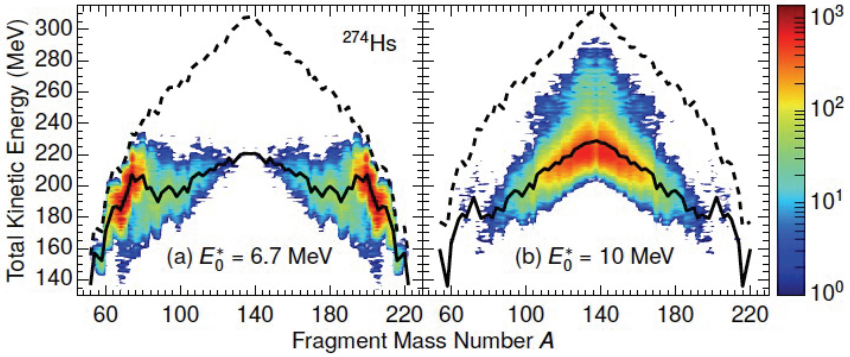

Figure 4. Same as Fig.1 but for the super-heavy nucleus ^{274}Hs at excitation energies 6.7 MeV (left-hand part) and 10 MeV (right-hand part). The dashed lines show the Q^*-values of each reaction, and the solid lines show the calculated average average values of TKE. (From [11]).

2.3. Angular momentum generation in fission

At scission the excitation energies and the angular momenta of the two fission fragments are statistically obtained. Assuming angular momenta of both fragments to be perpendicular to the axis connecting the fragments [8] (balanced by a collective rotation of the scissioning nucleus), the distribution of angular momenta of each fragment in the Fermi gas model is given by $F(I) = (2I+1)\frac{1}{\sqrt{8\pi}\sigma^3} exp\left(-\frac{I(I+1)}{2\sigma^2}\right)$, with the spin-cut off factor $\sigma^2 = TJ$, where $T = \sqrt{E_{exc}/a}$ is the temperature, a the level-density parameter and J is the moment of inertia. Consequently, for each fragment at scission the average angular momentum relates to the excitation energy as $\langle I\rangle_{H/L} \sim \sigma \sim E^{1/4}_{exc,H/L}$. Since the average neutron multiplicity $\bar{\nu}$ depends on available excitation energy of the fragment one expects $\langle I\rangle_{H/L} \sim \bar{\nu}^{1/4}_{H/L}$.

Based on these arguments the relation between the average angular momentum and the average neutron multiplicity can be estimated. If we assume a typical neutron binding energy of 6 MeV and a neutron kinetic energy of 1 MeV the total excitation energy at fission may be approximated as $\mathrm{TXE}_{H/L} \approx (6+1)\bar{\nu}_{H/L}$. But TXE=$E_{exc} + E_{dist}$, where the distortion energy E_{dist} is obtained as the energy gain as the shape of the fission fragment relaxes to equilibrium deformation.

The distortion energy does not contribute to the temperature related to the statistical angular momentum distribution at scission. In previous Metropolis calculations the excitation energy at scission was found to be around 80% of the total excitation energy and the distortion energy about 20% with some minor variations with mass number [4]. Assuming this relation for all fragment mass numbers and applying standard parameters for the moment of inertia (assuming rigid-body rotation and accounting for the relative orbital angular momentum) as well for the level-density parameters we obtain the simple relation [5]

$$\langle I\rangle_{H/L} = 0.38 A^{7/12} \bar{\nu}^{1/4}_{H/L}. \quad (1)$$

Utilising this relation with measured average neutron multiplicities for ^{238}U(n,f) [12] and for ^{252}Cf(SF) [13] we obtain the variation in average angular momentum with fragment mass number as shown in Fig. 5a) and b). The simple estimate gives a quite good agreement with data from Wilson *et al.* [9]. If instead it is assumed that the excitation energy at scission is 20% of the TXE (instead of 80%) a reduction with $4^{1/4}$ of $\langle I\rangle$ is obtained, see Fig. 5a) and b).

These simple arguments suggest first steps towards an explanation of the observed strong correlation between the saw-tooth structure of average angular momenta and the saw-tooth structure of the average neutron multiplicity [5]. Note that in order to obtain the saw-tooth variation of the angular momentum with fragment mass as a statistical effect requires that a sufficient part of the total excitation energy appears at scission, thus limiting the contribution to TXE from the distortion energy. Fission models where the total excitation energy is fully

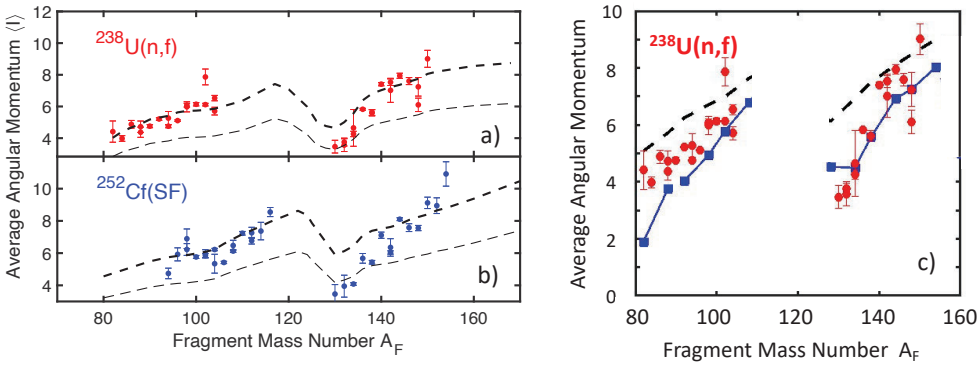

Figure 5. Average angular momentum of fission fragment with mass number A_F for a) ^{238}U(n,f) and for b) ^{252}Cf(SF). Data [9] are shown by circles, and calculations in the Fermi gas model by dashed lines. Thick and thin dashed lines assume that 80% and 20%, respectively of the total excitation energy emerges from the intrinsic energy. c) Calculated average angular momentum from microscopic level densities (blue squares) are compared to data [9] (red circles). Same excitation energies as in a) are used in the calculations. Fermi gas model results are shown by the dashed curves. (Partly from [5]).

generated from the deformation relaxation (e.g. [14]) provide no direct connection between the saw-tooth variation of angular momentum and neutron multiplicity.

Fig. 5c) shows results from microscopic calculations where shell structure in the level density is accounted for (see [5] for details), comparing well to data. Shell structure plays an important role in the obtained $\langle I \rangle$ values at different mass numbers. For example the shell gaps around ^{132}Sn imply a relatively small $\langle I \rangle$. A general lowering of the microscopic result compared to the Fermi gas result seen in Fig. 5c) is due to pairing.

3. Summary

Shell structure in fission is shown to play an important role in the appearance of a super-short mode in nuclei around ^{264}Fm and a super-asymmetric mode in SHE where the heavy fragments center around ^{208}Pb. In both cases the specific fission mode is fragile and changes as the excitation energy is slightly increased, with huge consequences on several observables. The observed [9] saw-tooth dependence of fragment angular momentum with mass number is understood in terms of a statistical generation of angular momentum at scission where shell structure is important.

Acknowledgements

S.Å. thanks the Royal Physiographical Society in Lund for financial support.

[1] J. Randrup and P. Möller, Phys. Rev. Lett. **106**, 132503 (2011).
[2] H. Uhrenholt *et. al.*, Nucl. Phys A **913**, 127 (2013).
[3] D.E. Ward *et. al.*, Phys. Rev. C **95**, 024618 (2017).
[4] M. Albertsson *et. al.*, Phys. Lett. **803**, 135276 (2020).
[5] T. Døssing *et. al.*, in preparation.
[6] P. Möller *et. al.*, Phys. Rev. C **79**, 064304 (2009).
[7] M. Albertsson *et. al.*, Phys. Rev. C **104**, 064616 (2021).
[8] J.B. Wilhelmy *et. al.*, Phys. Rev. C **5**, 2041 (1972).
[9] J.N. Wilson *et. al.*, Nature **590**, 566 (2021).
[10] M. Albertsson *et. al.*, Eur. Phys. J. A **56**, 46 (2021).
[11] M. Albertsson *et. al.*, in preparation.
[12] F. Vives *et. al.*, Nucl. Phys. A **662**, 63 (2000).
[13] A. Göök *et. al.*, Phys. Rev. C **90**, 064611 (2014).
[14] B.D. Wilkins, E.P. Steinberg and R.R. Chasman, Phys. Rev. **C 14**, 1832 (1976).